



ELSEVIER

Contents lists available at ScienceDirect

Journal of Computational Physics

journal homepage: www.elsevier.com/locate/jcp

Short Note

On the properties and limitations of the height function method in two-dimensional Cartesian geometry

G. Bornia^a, A. Cervone^a, S. Manservigi^a, R. Scardovelli^{a,*}, S. Zaleski^b^a DIENCA – Lab. di Montecuccolino, Università degli Studi di Bologna, Via dei Colli 16, 40136 Bologna, Italy^b Institut Jean Le Rond d'Alembert (IJLRDA), UMR 7190, Université Pierre et Marie Curie – Paris 6 and CNRS, 4 place Jussieu, 75252 Paris Cedex 05, France

ARTICLE INFO

Article history:

Received 13 January 2010

Received in revised form 16 September 2010

Accepted 17 November 2010

Available online xxx

Keywords:

Interface reconstruction

VOF/PLIC method

Quadratic reconstruction

Height function

Normal vector

Curvature

ABSTRACT

In this study we define the continuous height function to investigate the approximation of an interface line and its geometrical properties with the height function method. We show that in each mixed cell the piecewise linear interface reconstruction and the approximation of the derivatives and curvature based on three consecutive height function values are second-order accurate. We also discuss the quadratic reconstruction and fourth-order accurate expressions of the normal and curvature. We present a hierarchical algorithm to compute the normal vector and curvature of an interface line with the height function method that switches automatically between second- and fourth-order approximations and that can be applied also when the local radius of curvature is of the order of the grid spacing.

© 2010 Elsevier Inc. All rights reserved.

1. Introduction

The correct representation of an interface and its geometrical properties plays a key role in the numerical simulation of physical phenomena which are also very important for industrial applications, such as multi-phase systems and free-surface flows. A precise calculation of the interface geometry is required to avoid a poor representation of singular surface forces, such as the capillary force, that may lead to unphysical flows around the interface and its unrealistic deformation followed by an eventual numerical breakup. The Volume-of-Fluid (VOF) method is a very popular technique to deal with the time evolution of interfaces in two-phase flows [1–3]. It is based on the phase indicator or characteristic function $\chi(\mathbf{x}, t)$, a multidimensional Heaviside step function with value 1 in the phase assumed to be the reference one, and 0 in the other phase or vacuum. The gradient of the function χ defines the outward unit normal \mathbf{n} , $\nabla\chi = -\mathbf{n}\delta_S$, with the surface distribution δ_S defined by the Dirac delta function [4]. The mean curvature κ is given by the spatial variation of the normal vector, $\kappa = -\nabla_S \cdot \mathbf{n}$, where the operator $(\nabla_S \cdot)$ denotes the surface divergence [5].

The color function or volume fraction C is the discrete version of χ and represents the fraction of each cell of the mesh which is occupied by the reference phase

$$C_n(t) = \frac{1}{V_n} \int_{V_n} \chi(\mathbf{x}, t) d\mathbf{x}, \quad (1)$$

where V_n is the volume of the n th cell. The spatial variations of the volume fraction function are far from being smooth and to compute its derivatives a “mollified” \tilde{C} function is often used. It can be obtained by a repeated application of a simple

* Corresponding author. Tel.: +39 051 6441720; fax: +39 051 6441747.

E-mail addresses: ruben.scardovelli@unibo.it, raus@mail.ing.unibo.it (R. Scardovelli).

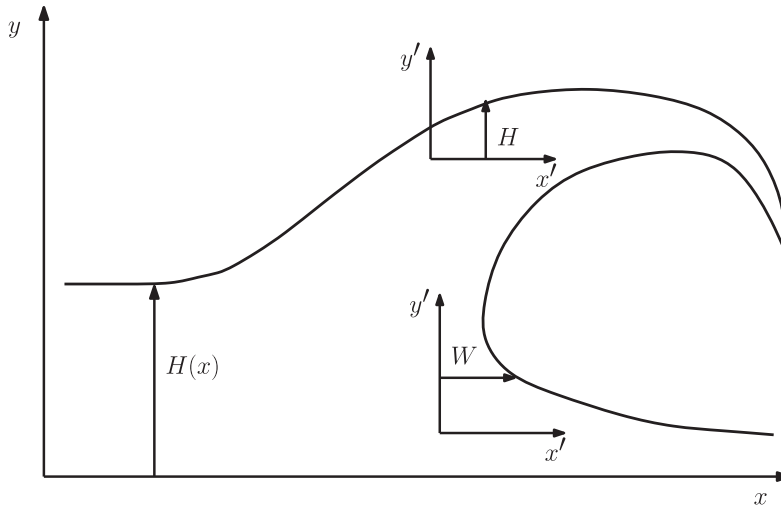


Fig. 1. If the height function $H(x)$ is defined with respect to a fixed coordinate system it cannot represent a multi-valued interface line. With a local coordinate system the function is again single-valued and we can choose between a local vertical height H and a horizontal width W .

diffusion or Laplacian operator [6] or the convolution of the C function with a smoothing kernel [7–9]. With the more regular \tilde{C} function we can also extend the normal away from the interface and replace the surface operator ∇_S with the three-dimensional operator ∇ [7], then $\mathbf{n} = -\nabla\tilde{C}/|\nabla\tilde{C}|$ and $\kappa = -\nabla \cdot \mathbf{n}$. However, as we refine the grid the numerical approximation of the first derivative based on these techniques is not able to reproduce the Dirac delta function and the curvature computation may not even converge [10].

Alternatively we can compute the interface geometrical properties from the C distribution with the height function approach [11,12], without going across the discontinuity of the function χ . In two dimensions and in its simplest formulation, the height function represents the distance of the points of the interface line from a reference coordinate axis and is restricted to single-valued functions of one independent variable, as shown in Fig. 1. This feature limits the possibility to follow the full non-linear evolution of an unstable wave: we have to stop the simulation when the interface “overhangs” and becomes a multi-valued function. However, we are not obliged to consider a fixed coordinate system throughout the whole computational domain and we can use local coordinate systems moving along the grid lines of a Cartesian mesh to define a local height H along the vertical coordinate or a width W in the horizontal direction (see again Fig. 1). The height H is proportional to the sum of the volume fractions in the vertical direction and three consecutive values of H are needed to estimate its first and second derivatives with finite differences. A moving stencil in a two-dimensional Cartesian grid is then based on a $3 \times n$ block of cells, where the fixed values $n = 3, 5, 7$ have been considered in the literature [10,13–15]. Algorithms with a variable stencil height n have also been proposed more recently [16,17]. There are also widely-used reconstruction algorithms, such as the ELVIRA algorithm [18] and the centered columns scheme [18,19], that are implicitly based on the notion of the height function.

The height function method has been shown, both analytically and numerically, to provide second- and fourth-order accurate approximations of the normal and curvature in uniform and nonuniform Cartesian grids [20,21]. In this note we define the continuous height function and derive again these approximations in grids with square cells together with analytical expressions for the approximation errors. We also show that the piecewise linear and quadratic reconstructions are respectively second-order and third-order accurate. We then present a hierarchical algorithm to compute the geometrical properties of the interface line. The algorithm calculates the local normal and curvature by using consecutive values of H or W , and only when this is not possible it combines height and width data. A similar algorithm, even if limited to curvature calculation, has been presented recently [17], but at low resolution we extend the method by fitting the height function (HF) points with the approximated osculating circle rather than a parabolic least-squares fit. Moreover, for particular alignments of the interface with respect to the grid lines we compute the normal by interpolating the normal vector of the surrounding cells [22], and we extend the procedure to the curvature as well. However, our interpolation is based on quadratic polynomials which are shown to be second-order accurate, rather than a local linearization of the interface line. Finally, we present numerical results to validate our algorithm.

2. The continuous height function approximation of an interface line

We consider an interface line described by the implicit equation $s(x,y) = 0$ that locally we can write in the explicit form $y = f(x)$, when $|df(x)/dx| \leq 1$, or with the inverse form $x = f^{-1}(y)$, when $|df^{-1}(y)/dy| < 1$. Furthermore, we assume that the function $f(x)$ and its derivatives are continuous, with $f^{(n)}(x) = d^n f(x)/dx^n$. Let the parameter h be the grid spacing. We define the continuous height function $H(x; h)$ as

$$H(x; h) = \frac{1}{h} \int_{x-h/2}^{x+h/2} f(t) dt, \quad (2)$$

i.e. the mean value of the function in $[x - h/2, x + h/2]$. If we consider a primitive, or integral function, $F(x)$ of $f(x)$, then $H(x; h) = (F(x + h/2) - F(x - h/2))/h$. We take the difference $f(x) - H(x; h)$ and expand it in Taylor series in the small parameter h to get

$$f(x) - H(x; h) = -\frac{f^{(2)}(x)}{24} h^2 + \mathcal{O}(h^4). \quad (3)$$

Thus, the height function is a second-order accurate approximation of the original function if we assume that the fourth derivative of $f(x)$ in the remainder is bounded. If the fourth derivative is continuous and limited from above, then the convergence is uniform. When the absolute value of the remainder is smaller than that of the second-order term, the point with coordinates (x, H) lies above the graph of the function when $f(x)$ is convex, i.e. $f^{(2)}(x) > 0$, and below it when concave. This condition on the absolute value is clearly sufficient but not necessary.

We now let $H_n = H(x + nh; h)$ and consider the five consecutive height points with coordinates (nh, H_n) , with $n = (0, \pm 1, \pm 2)$, centered around $H_0 = H(x; h)$. We then approximate with finite differences the second derivative in (3) to define the corrected height function $H^c(x; h) = H_0 - (H_{+1} + H_{-1} - 2H_0)/24$. By expanding in Taylor series the difference $f(x) - H^c(x; h)$ we get

$$f(x) - H^c(x; h) = \frac{3f^{(4)}(x)}{640} h^4 + \mathcal{O}(h^6). \quad (4)$$

H^c is a fourth-order accurate estimate of the original function $f(x)$ and when its second and fourth derivatives have the same sign the two points (x, H) and (x, H^c) are on opposite sides of the interface line.

We can approximate the first and second derivatives $f^{(1)}(x)$ and $f^{(2)}(x)$ and the curvature $\kappa(x) = -f^{(2)}(x)/[1 + (f^{(1)}(x))^2]^{3/2}$ by defining the continuous functions

$$H^{(1)}(x; h) = \frac{H_{+1} - H_{-1}}{2h}, \quad (5)$$

$$H^{(2)}(x; h) = \frac{H_{+1} + H_{-1} - 2H_0}{h^2}, \quad (6)$$

$$\kappa_p(x; h) = -\frac{H^{(2)}(x; h)}{[1 + (H^{(1)}(x; h))^2]^{3/2}}, \quad (7)$$

then with an expansion in Taylor series we obtain

$$f^{(1)}(x) - H^{(1)}(x; h) = -\frac{5f^{(3)}(x)}{24} h^2 + \mathcal{O}(h^4), \quad (8)$$

$$f^{(2)}(x) - H^{(2)}(x; h) = -\frac{f^{(4)}(x)}{8} h^2 + \mathcal{O}(h^4), \quad (9)$$

$$\kappa(x) - \kappa_p(x; h) = \frac{S(x)f^{(4)}(x) - 5T(x)}{8S^{5/2}(x)} h^2 + \mathcal{O}(h^4), \quad (10)$$

with $S(x) = 1 + (f^{(1)}(x))^2$ and $T(x) = f^{(1)}(x)f^{(2)}(x)f^{(3)}(x)$. The approximation of the derivatives and curvature of the function $f(x)$ with the height function H and centered finite differences is second-order accurate with the grid spacing h . It is straightforward to show that the forward and backward approximations are both first-order accurate.

We can also consider the circle through the three consecutive points $(-h, H_{-1})$, $(0, H_0)$ and (h, H_{+1}) . As a matter of fact, this is a numerical approximation of the osculating circle at point $(x, f(x))$. The signed curvature $\kappa_c(x; h)$ of the circle, negative when the function $f(x)$ is convex and positive when it is concave, is

$$\kappa_c(x; h) = -\frac{2h(H_{-1} - 2H_0 + H_{+1})}{\left((h^2 + \Delta H_{(0,-1)}^2) (4h^2 + \Delta H_{(-1,+1)}^2) (h^2 + \Delta H_{(0,+1)}^2) \right)^{1/2}}, \quad (11)$$

with $\Delta H_{(l,m)}^2 = (H_l - H_m)^2$. The expansion of the difference between $\kappa(x)$ and its approximation shows that $\kappa_c(x; h)$ is also second-order accurate

$$\kappa(x) - \kappa_c(x; h) = \frac{U(x)}{8S^{7/2}(x)} h^2 + \mathcal{O}(h^4), \quad (12)$$

where $U(x)$ is an algebraic expression containing the derivatives of $f(x)$ up to fourth order. Similar expressions are obtained with the corrected height function H^c , but with different coefficients, for example in (8) the coefficient $5/24$ is replaced by $1/6$.

The approximation of the first and second derivatives of $f(x)$ with H^c requires five consecutive values of H . With these five values we can also derive expressions for the first two derivatives of $f(x)$ that are fourth-order accurate. To this aim, we need to define the following continuous functions that approximate the third and fourth derivatives

$$H^{(3)}(x; h) = \frac{-H_{-2} + 2H_{-1} - 2H_{+1} + H_{+2}}{2h^3}, \quad (13)$$

$$H^{(4)}(x; h) = \frac{H_{-2} - 4H_{-1} + 6H_0 - 4H_{+1} + H_{+2}}{h^4}. \quad (14)$$

By substituting (13) in (8) we get the following approximation of the first derivative

$$\tilde{H}^{(1)}(x; h) = \frac{34(H_{+1} - H_{-1}) - 5(H_{+2} - H_{-2})}{48h}. \quad (15)$$

For the curvature we combine the definition (7) of κ_p and the first term on the r.h.s. of (10) and substitute the centered finite differences approximation of the derivatives up to fourth order to get $\tilde{\kappa}_p(x; h) = N(x)/M(x)$, where

$$N(x) = -2h \left[2h^2 (12(H_{-1} + H_{+1}) - (H_{-2} + 22H_0 + H_{+2})) + (H_{-1} - H_{+1})((H_{-1} - H_{+1})(H_{-1} + H_{+1} - H_0) + H_{+2}(5H_0 - 3H_{-1} - 2H_{+1}) - H_{-2}(5H_0 - 2H_{-1} - 3H_{+1})) \right],$$

$$M(x) = \left[4h^2 + (H_{-1} - H_{+1})^2 \right]^{5/2}.$$

We finally expand in Taylor series the difference between the first derivative and curvature and the respective approximations $\tilde{H}^{(1)}(x; h)$ and $\tilde{\kappa}_p(x; h)$

$$f^{(1)}(x) - \tilde{H}^{(1)}(x; h) = \frac{259f^{(5)}(x)}{5760}h^4 + \mathcal{O}(h^6), \quad (16)$$

$$\kappa(x) - \tilde{\kappa}_p(x; h) = \frac{V(x)}{1920S^{7/2}(x)}h^4 + \mathcal{O}(h^6), \quad (17)$$

where $V(x)$ is an algebraic expression containing the derivatives of $f(x)$ up to sixth order. The estimates $\tilde{H}^{(1)}(x; h)$ and $\tilde{\kappa}_p(x; h)$ are clearly fourth-order accurate.

3. The discrete height function and the interface reconstruction

3.1. Initialization of the volume fraction and of the discrete height function

To initialize the volume fraction C in a grid cell (i, j) one can determine the intersections of the interface equation with the cell boundary and then compute the area comprised between the interface and the boundary either analytically or numerically. If the interface does not cut the boundary, the cell is either empty, C is zero, or full, C is unity. The discrete heights or widths are then calculated by adding columnwise or rowwise the C data. Starting from the cut cell (i, j) , the local height H is defined as

$$H = \frac{1}{h} \int_{x_i-h/2}^{x_i+h/2} f(t) dt = \frac{1}{h} \sum_{k=-n}^n C_{i,j+k} h^2, \quad (18)$$

where the values $n = 1, 2, 3$ have been widely used in the literature, corresponding to a one-dimensional stencil with 3, 5 and 7 cells, respectively. The height H is located in the i th column but it is not necessarily inside the cell (i, j) . Furthermore, the definition (2) of the continuous height requires that the interface line crosses the column of thickness h centered at abscissa x .

Remark 1. If we reconstruct the interface from the C data we can ensure this requirement only when the sequence of mixed cells in the stencil is bounded by a full cell on one side and an empty one on the other side.

In the example of Fig. 2, and in the quadrant with $x \geq 0$ and $y \geq 0$, we can define the heights and widths shown in Fig. 2(b). In the first two columns three vertical cells are required to compute the value of H , four cells are required in the third column, because there are two consecutive mixed cells, but in the fourth column with the dashed height it is not possible to place the computed value anywhere.

In this study we initialize the C data numerically. The interface line is given analytically by the implicit equation $s(x, y) = 0$ together with its partial derivatives $\partial s / \partial x$ and $\partial s / \partial y$. The algorithm checks the sign of the implicit function on discrete points along the boundary of the square grid cells of side h . The distance between two consecutive points is a free parameter, say $h/20$, and interface structures smaller than this value may not be detected. If the sign does not change, the cell is either full or empty and it is assumed that the characteristic function is unity in the region where $s(x, y) < 0$. If the sign changes we have a

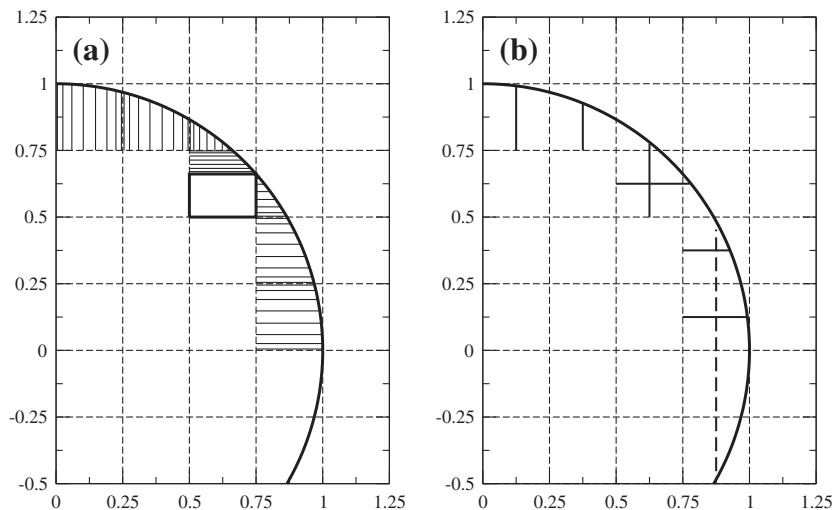


Fig. 2. (a) Subdivision of mixed cells and ordinates to compute the volume fraction data with a Gauss integration, in the quadrant $x \geq 0, y \geq 0$; (b) heights and widths in the same quadrant. The dashed height in the fourth column is computed with the volume fraction data, but cannot be placed in any cell.

mixed cell, the intersections between the interface and the cell boundary are then computed and the cell is further subdivided in rectangles either full or empty or with the interface. In the last case we compute the area with a negative value of s with a Gauss integration with 8 nodes. The ordinates are calculated along the coordinate axis with the maximum absolute value of the partial derivative of $s(x, y)$. In the example of Fig. 2(a) we show the mesh and the ordinates used to compute the volume fraction field in the positive quadrant, for a circular sector with radius $r = 1$ and $r/h = 4$. For this case the area difference between the analytical value $\pi/4$ and the computed one is of the order of machine accuracy.

To compute the discrete heights we use (18) and a variable stencil [16,17], which is centered at the mixed cell (i, j) and with a maximum length of n_c cells (we usually set $n_c = 7$). Since the algorithm is dynamical, the summation in (18) stops as soon as a full cell and an empty one are found on opposite sides of the stencil. The height H , or the width W , is stored as an offset from the cell center together with a positive integer flag to indicate if the height is measured from the top or bottom of the cell. Because of this memorization, when we collect the heights we need to translate them to a common origin before computing the derivatives. More than one mixed cell can be found in the same stencil, for example in the third column of Fig. 2(b), but only one will contain the height H . In the mixed cells with no height, the flag is set to a negative value to indicate that an interpolation of the local geometrical data is required in that cell. Finally, at small resolutions there may be a very limited number of mixed cells that do not contribute to the calculation of the height H or width W (in Fig. 5(a) these are the four mixed cells that share only a vertex with the full central cell). In these *isolated* cells we consider the mid-point of the Parker–Youngs reconstruction segment [23].

3.2. A hierarchical approach for the normal and curvature computation and geometrical data interpolation

We have defined the height function points in the computational domain and we can now calculate the local values of the interface normal and curvature with the finite difference expressions we have previously derived. In particular, the normal vector \mathbf{n} is perpendicular to the local tangent, whose slope is equal to $f^{(1)}(x)$, and has the same accuracy of the first derivative computed with the HF method. Let us suppose that the cell (i, j) contains the discrete height H , we then look for another height in the two neighboring columns with indices $i - 1$ and $i + 1$. The one-dimensional search is centered around the row with index j with a stencil with five cells. When we find two neighboring heights we define the three height points $(-h, H_{-1}), (0, H_0), (h, H_{+1})$ of Fig. 3(a) and also check the two columns with indices $i - 2$ and $i + 2$. If this second search is also successful we define two additional height points and consider the fourth-order scheme to compute the first derivative and the curvature, otherwise we use the second-order one. On the other hand if the search for three consecutive heights fails, we combine heights and widths.

This last case occurs more often where $|f^{(1)}(x)| \approx 1$ and the local radius of curvature is only a few times the grid spacing h . In the example of Fig. 2(b) the height is defined in the first three columns but not in the fourth one, where three widths are however found. If we consider the third column as the central one, we can define the two height points $(-h, H_{-1})$ and $(0, H_0)$, but not the right one. In this case we select the first width W that we find in the stencil with five vertical cells, that is centered at row j where H_0 is located, with the sequence $j + n$ and $n = 0, -1, 1, -2, 2$. The ordinate y of the width W defines the height H_{+1} of the right point, but the width W is usually not in the middle of the column, hence it defines an abscissa $h_+ \neq h$. In the most general case, we may end up collecting three points $(-h_-, H_{-1}), (0, H_0)$ and (h_+, H_{+1}) , with $h_- \neq h_+ \neq h$, and calculate the tangent slope and the curvature from the circle through these three points. For example the curvature is given by the following expression that generalizes (11)

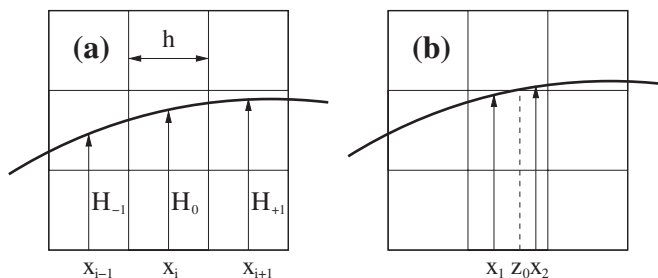


Fig. 3. Interface line in a computational grid with square cells of side h : (a) the interface intersects two consecutive vertical grid lines in the same cell, the height function and its derivatives are calculated in the midpoint x_i ; (b) here the intersections are in two different cells and the normal and curvature must be interpolated in the two midpoints x_1 and x_2 .

$$\kappa_C(x; h) = -\frac{2(h_+H_{-1} - (h_- + h_+)H_0 + h_-H_{+1})}{\left(\left(h_-^2 + \Delta H_{(0,-1)}^2\right)\left(h_+^2 + \Delta H_{(0,+1)}^2\right)\left((h_- + h_+)^2 + \Delta H_{(-1,+1)}^2\right)\right)^{1/2}}. \quad (19)$$

It is straightforward to show that the approximations (5), and (6) compute the coefficients of the parabola $y = ax^2 + b x + c$ through three evenly-spaced heights, where $2a = H^{(2)}$, $b = H^{(1)}$, $c = H_0$. When we combine heights and widths we allow $h_+ \neq h$, then if we let h_+ go to zero along the width W as shown in Fig. 4, the local radius of curvature of the interface line decreases and the point H_{+1} does not move to H_0 . In these conditions, the parabolic approximation does not converge, while the circular fit remains well-behaved. As an alternative approach it is possible to collect all heights and widths in the 3×3 block of cells centered at point (i, j) and if their number is greater than 4 to fit a parabola with a least-squares technique. This approach has been also extended to three dimensions [17].

Remark 2. When the heights are unevenly spaced we compute the tangent and the curvature from the circle through the three points.

Remark 3. By combining heights and widths we can extend the HF method below the typical resolution of $\rho/h \approx 5$ (as depicted in Fig. 2(b)), where ρ is the local radius of curvature of the interface line.

However, heights and widths correspond to different representations of the same function and if we substitute one for the other in the finite difference approximation of the derivatives we systematically introduce an error. If this error is $\mathcal{O}(h^2)$, then the error for $H^{(2)}$ is $\mathcal{O}(1)$. This is actually what we have found in the development of the algorithm when we have mixed the two representations where $|f^{(1)}(x)| \approx 1$, at all resolutions. In this region, the numerical approximation of the curvature of a circle is roughly constant with h and does not converge. Therefore, in the hierarchical approach we first check for three (five) consecutive values of the HF, in this way the algorithm is second-order (fourth-order) accurate as h goes to zero. When this is not possible, we combine heights and widths to compute the approximated osculating circle which sets a lower limit for the local radius of curvature, $\rho/h \approx 1$.

Once we have calculated the normal and curvature at the height points, we need to check if data interpolation is required. In Fig. 3(a) the two intersections at $x_i - h/2$ and $x_i + h/2$ of the interface with the vertical grid lines are in the same cell and the abscissa x_i of the height, its first derivative and curvature are located in the middle of the i th column. For this case no interpolation is required. In Fig. 3(b) the interface line has been shifted in the vertical direction, the two intersections are now in different cells and we need to compute the first derivative and the curvature in the two midpoints x_1 and x_2 . It is straightforward to show that the parabola through three consecutive height function points provides a second-order accurate estimate of the first derivative in the i th column, but the second derivative is only first order. Therefore, we consider the two quadratic polynomials $P_{f^{(1)}}(x; h)$ and $P_{\kappa}(x; h)$, constrained by three consecutive estimates of the first derivative and curvature, respectively. For any point $x = x_i + \gamma h$ with $|\gamma| < 1/2$ we find

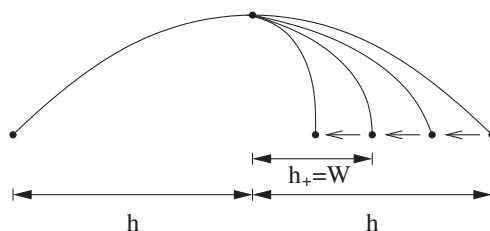


Fig. 4. The right point moves along the width W as h_+ goes to zero and the local radius of curvature decreases. The circle fit remains well-behaved, but not the parabolic fit.

$$f^{(1)}(x) - P_{f^{(1)}}(x; h) = -\frac{5f^{(3)}(x_i)}{24}h^2 + \frac{\gamma(4\gamma^2 - 9)f^{(4)}(x_i)}{24}h^3 + \mathcal{O}(h^4), \quad (20)$$

$$\kappa(x) - P_\kappa(x; h) = \frac{S(x_i)f^{(4)}(x_i) - 5T(x_i)}{8S^{5/2}(x_i)}h^2 + \mathcal{O}(\gamma h^3), \quad (21)$$

when the interpolated values are second-order accurate. If all of them are fourth order we get

$$f^{(1)}(x) - P_{f^{(1)}}(x; h) = \frac{\gamma(\gamma^2 - 1)f^{(4)}(x_i)}{6}h^3 + \mathcal{O}(h^4), \quad (22)$$

$$\kappa(x) - P_\kappa(x; h) = \frac{Z(x_i; \gamma)}{6S^{5/2}(x_i)}h^3 + \mathcal{O}(h^4), \quad (23)$$

where $Z(x_i; \gamma)$ is an algebraic expression containing the derivatives of the function $f(x)$ up to fifth order and the powers of γ . In this case the interpolated values are only third-order accurate with the grid spacing h .

In the numerical implementation we first check if an interpolation is required by considering the value of the integer flag in two adjacent cells. If this is the case, we gather three consecutive values of the height, first derivative and curvature. The parabola through the heights is used to estimate the intersection point z_0 of Fig. 3(b), while the abscissa of the midpoint x_1 , or x_2 according to the flag value, is used to compute the first derivative and curvature from the respective parabolic fit. The structure of the interpolation routine is also hierarchical, we first look for data obtained either from heights or widths, only when they are not found we mix the two different representations and in this case the interpolation is only linear.

The computation in three dimensions of the height function, its partial derivatives with finite differences and the osculating sphere is more involved, but straightforward. On the other hand, in the interpolation routine the determination of the two points that substitute x_1 and x_2 of Fig. 3(b), will certainly require some careful analysis and approximation.

3.3. Convergence analysis of the reconstruction

In our discussion of the HF method, the computation of the normal and curvature in the mixed cells has not been linked to the reconstruction of the interface, which however plays a major role in the propagation of the interface and in particular in the determination of the reference phase fluxes through the cell boundary: the better the reconstruction, the smaller the numerical deformation of the interface line in the propagation. We first examine the usual linear reconstruction and then briefly discuss a possible parabolic approximation.

Let us consider a characteristic function $\chi(x, y, t)$ and the associated C data at time t_0 in a two-dimensional domain Ω partitioned with square cells of side h . A VOF algorithm reconstructs the interface line with a piecewise linear approximation and defines a different function $\tilde{\chi}(x, y, t_0)$. A natural measure of the reconstruction error in L_1 norm is [18]

$$E_1 = \frac{1}{A} \int_{\Omega} |\chi(x, y, t_0) - \tilde{\chi}(x, y, t_0)| dx dy, \quad (24)$$

where A is a suitable normalization constant, for example the line length. Any VOF reconstruction is at least first order with this norm. To show this, we subdivide the interface line in M sections where we consider either the explicit form $y = f(x)$, when $|f^{(1)}(x)| \leq 1$, or $x = f^{-1}(y)$. Let us consider the k th section where $y = f(x)$, and a vertical stripe with n_k consecutive columns of thickness h , that covers the interface section. Since $|f^{(1)}(x)| \leq 1$ the local portion of the line in each vertical column is inside one or two cells, therefore the k th section is contained in $2n_k$ cells with area $2hL_k$, where $L_k = n_k h$. Moreover, in each mixed cell the area difference between the χ distribution and the approximated $\tilde{\chi}$ is bounded by the cell area itself, then the term $2h \sum_{k=1}^M L_k$, which is linear in h , is an upper bound for the integral in (24).

It is straightforward to show that the linear HF reconstruction is second-order accurate with (24). We limit our discussion to only one of the M sections and consider first a single column of thickness h centered at x_i , then $H_0 = H(x_i; h)$. The HF approximation is the straight line $y = g_i(\gamma h) = b_i \gamma h + c_i$, where $-1/2 \leq \gamma \leq 1/2$, $b_i = (H_{+1} - H_{-1})/2h$, and $c_i = H_0$ by the area conservation constraint. We limit the integral in (24) to this column, expand the function $f(x)$ in Taylor series around x_i and the height functions in the parameter h to obtain

$$\int_{-1/2}^{1/2} |f(x_i + \gamma h) - g_i(\gamma h)| h d\gamma = \frac{|f^{(2)}(x_i)|}{18\sqrt{3}} h^3 + \mathcal{O}(h^4), \quad (25)$$

with $x = x_i + \gamma h$. Finally we sum the contribution from the n_k columns and use the mean value theorem in the form $\sum_{i=1}^{n_k} |f^{(2)}(x_i)| = n_k |f^{(2)}(\xi)|$, where ξ is an abscissa in the k th section of length L_k and $n_k h = L_k$, to get

$$E_1 = \frac{L_k}{A} \frac{|f^{(2)}(\xi)|}{18\sqrt{3}} h^2 + \mathcal{O}(h^3). \quad (26)$$

The linear reconstruction is pointwise second-order accurate in the column and it is usually not continuous across its boundary. To analyse this issue we also consider the reconstruction in the next column, $y = g_{i+1}(\gamma h) = b_{i+1} \gamma h + c_{i+1}$, where

$b_{i+1} = (H_{+2} - H_0)/2h$ and $c_{i+1} = H_{+1}$. We compute the value of the linear approximations and of the original function on the boundary abscissa and with an expansion in Taylor series we get

$$g_i\left(\frac{h}{2}\right) - g_{i+1}\left(-\frac{h}{2}\right) = \frac{1}{4}f^{(3)}(x_i)h^3 + \mathcal{O}(h^4), \tag{27}$$

$$g_i\left(\frac{h}{2}\right) - f\left(x_i + \frac{h}{2}\right) = -\frac{1}{12}f^{(2)}(x_i)h^2 + \mathcal{O}(h^3) = -\frac{1}{12}\beta\kappa h^2 + \mathcal{O}(h^3), \tag{28}$$

$$g_{i+1}\left(-\frac{h}{2}\right) - f\left(x_i + \frac{h}{2}\right) = -\frac{1}{12}f^{(2)}(x_i)h^2 + \mathcal{O}(h^3) = -\frac{1}{12}\beta\kappa h^2 + \mathcal{O}(h^3), \tag{29}$$

where the coefficient $\beta = (1 + (f^{(1)}(x_i))^2)^{3/2}$ satisfies $1 \leq \beta \leq 2\sqrt{2}$, since $|f^{(1)}(x)| \leq 1$, and κ is the local curvature. The two end points $g_i(h/2)$ and $g_{i+1}(-h/2)$ are closer to each other, $\mathcal{O}(h^3)$, than to the function point $f(x_i + h/2)$, $\mathcal{O}(h^2)$, as h goes to zero. They also lie on the same side as long as the curvature does not change its sign.

In the same column centered at x_i we now consider the parabolic approximation $y = g_i(\gamma h) = a_i(\gamma h)^2 + b_i\gamma h + c_i$, where $2a_i = H^{(2)}(x_i; h)$, $b_i = H^{(1)}(x_i; h)$ and $c_i = H^c(x_i; h)$. This line satisfies the area conservation requirement, it is fourth-order accurate in the cell center, $g_i(0) = H^c(x_i; h)$, but with the usual expansion in Taylor series it can be shown that it is only third-order accurate in the other abscissae of the column. In agreement with this result, when we substitute the parabola in (25) we get

$$\int_{-1/2}^{1/2} |f(x_i + \gamma h) - g_i(\gamma h)| h d\gamma = \frac{3|f^{(3)}(x_i)|}{64} h^4 + \mathcal{O}(h^5) \tag{30}$$

and

$$E_1 = \frac{L_k}{A} \frac{3|f^{(3)}(\xi)|}{64} h^3 + \mathcal{O}(h^4) \tag{31}$$

for the global error. At the cell boundary we now get

$$g_i\left(\frac{h}{2}\right) - g_{i+1}\left(-\frac{h}{2}\right) = \frac{1}{6}f^{(3)}(x_i)h^3 + \mathcal{O}(h^4), \tag{32}$$

$$g_i\left(\frac{h}{2}\right) - f\left(x_i + \frac{h}{2}\right) = \frac{1}{12}f^{(3)}(x_i)h^3 + \mathcal{O}(h^4), \tag{33}$$

$$g_{i+1}\left(-\frac{h}{2}\right) - f\left(x_i + \frac{h}{2}\right) = -\frac{1}{12}f^{(3)}(x_i)h^3 + \mathcal{O}(h^4). \tag{34}$$

These differences are all third-order accurate and from (33) and (34) the two end points are now on a different side with respect to the interface line. As a final remark we mention the possibility of a continuous parabolic reconstruction, but with a more complex algorithm and higher storage requirements. Notice that the point with coordinates $(h/2, R_i)$ on the right boundary of the i th column, with $R_i = (g_i(h/2) + g_{i+1}(-h/2))/2$, and the point $(-h/2, L_i)$ on the left boundary, with $L_i = (g_i(-h/2) + g_{i-1}(h/2))/2$, are both fourth-order accurate. It can be easily shown that the parabola through these two points and that satisfies the area conservation constraint is fourth-order accurate at $x = 0, \pm h/2$ and third-order accurate in the other abscissae. By construction the end point $(h/2, R_i)$ is shared with the neighboring right column, and $(-h/2, L_i)$ with the left one. Alternatively, one could couple the quadratic reconstruction based on the HF to some of the features of the Quadratic Spline based Interface (QUASI) algorithm [24] to enforce continuity of the line and of its first derivative at the cell boundary.

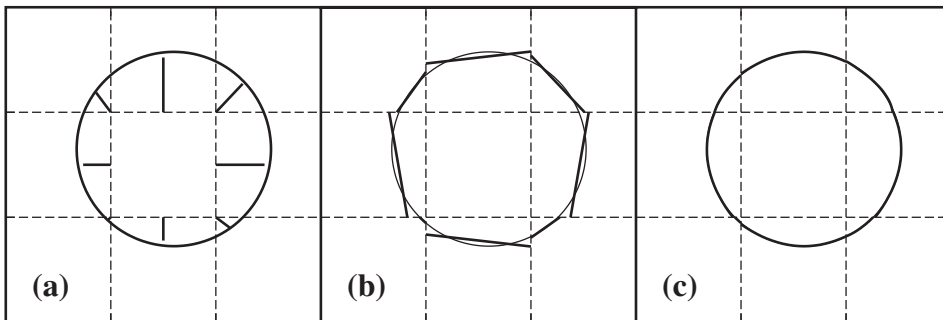


Fig. 5. (a) A circle with $r/h = 0.925$, with heights and widths, while the four diagonals connect to the midpoint of the Parker-Youngs reconstruction; (b) piecewise linear reconstruction with the hierarchical approach; (c) piecewise parabolic reconstruction with area conservation.

A few properties of the linear and quadratic reconstructions can be seen in the circle with $r/h = 0.925$ of Fig. 5(a), which still contains a full cell in its interior. The height function is defined in the four cells sharing a side with the full one; in the other four isolated mixed cells we consider the midpoint of the Parker–Youngs reconstruction segment. In all the cells we have to combine heights and widths to compute the interface properties: the curvature κ_c is calculated with (19) and the second derivative as $H^{(2)} = -\kappa_c[(1 + (H^{(1)})^2)^{3/2}]$. The piecewise linear reconstruction with the hierarchical approach is shown in Fig. 5(b): the approximation of the curved interface line is rather poor as in any other linear approximation. In Fig. 5(c) we show the piecewise quadratic reconstruction. In the cells with the height the parabola $y = ax^2 + bx + c$, with $2a = H^{(2)}$, $b = H^{(1)}$ and $c = H - h^2 H^{(2)}/24$, automatically satisfies the area conservation constraint, while in the other four diagonal cells we enforce it by keeping a and b fixed and changing c . Below this minimal resolution the HF points cannot be defined and the method has to be combined with some other approach.

4. Numerical results

In the previous section we have shown that the error of a parabolic reconstruction in a column of width h is proportional to the third derivative of $f(x)$. Therefore, for a parabolic interface its local normal and curvature can be computed exactly. In this section we discuss only the approximation of a circular interface with our hierarchical procedure, since the results obtained for a sinusoidal interface at the same resolution show a similar behavior [25]. We consider again the circular interface line, in the quadrant $x \geq 0$, $y \geq 0$ of Fig. 2, given by $y = f(x) = \sqrt{1 - x^2}$, together with its integral function $F(x) = [x\sqrt{1 - x^2} + \arcsin(x)]/2$. With $f(x)$ and $F(x)$ we compute the continuous functions H , $H^{(1)}$, $H^{(2)}$, κ_p and κ_c , defined in (2), (5)–(7) and (11). In the numerical algorithm we also set $n_c = 7$ as the maximum length of the stencil used to define the HF points.

We first present in Fig. 6 the results at high resolution, $r/h = 64$. We consider the height H in the range $0 \leq \alpha \leq 3\pi/8$, where α is the angle between the interface normal and the y -axis. The thick lines represent the analytical errors for the first derivative and curvature. In particular, the lower line in Fig. 6(a) represents the fourth-order error for the first derivative and it is computed analytically from the l.h.s. of (16). The upper line is the second-order error from the l.h.s. of (8). The full circles are the discrete errors computed from the given volume fraction field. Notice that by moving the center of the circle in the vertical direction we change the local value of the HF but not that of the derivatives, while by moving the center in the horizontal direction we simply compute different points of the analytical error lines. The squares are the errors at the points where we need data interpolation because the interface cuts two consecutive cells in the same column, as discussed in Section 3.2 and shown in Fig. 3(b).

For the first derivative we also draw two thin lines. The lower curve corresponds to the first term on the r.h.s. of (22) calculated at the cell boundary where $\gamma = 1/2$. It clearly represents an upper bound for the interpolation error when the first derivative data are fourth-order accurate. From (22) this error scales with the third power of h . The upper curve is the sum of the first two terms on the r.h.s. of (20) with $\gamma = 1/2$. This line is an accurate upper bound of the interpolation error when the data are second-order accurate. When $\alpha \approx \pi/4$ we observe a smooth transition between the two different

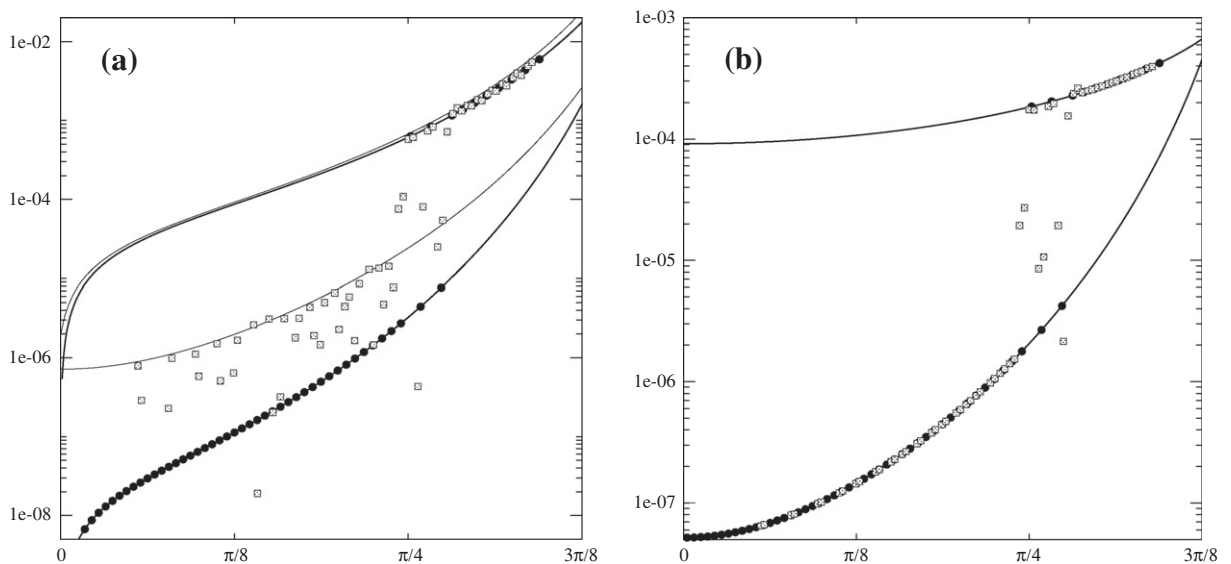


Fig. 6. Analytical errors (thick lines) with the continuous height function for a circle with $r/h = 64$ and $0 \leq \alpha \leq 3\pi/8$: (a) first derivative; (b) curvature. Top line is second-order accurate, bottom line is fourth-order accurate. Numerical errors from the volume fraction field are at the discrete HF points (full circles) and at the interpolated points (dotted squares). Thin lines in (a) are the first terms of the interpolation errors (20) and (22), respectively.

approximations of the first derivative. As a matter of fact, in this region a bigger value of n_c is required for the fourth-order approximation. However when $\alpha > \pi/4$, the width W provides an approximation which is fourth-order accurate and does not require a wider stencil. The error curves for W are obtained from the continuous lines in Fig. 6 with a simple mirror reflection around the axis $\alpha = \pi/4$. The choice between the two alternatives can be done in a very simple way by selecting the minimum absolute value of the first derivative. The results for the curvature are shown in Fig. 6(b). For a circular line the first term on the r.h.s. of (23) is identically zero and the interpolation error lines have not been drawn since they are very close to the two lines of Fig. 6(b).

In Fig. 7 we present the results for the circular sector at low resolution, $r/h = 4$. The analytical errors cannot be defined up to $\alpha = \pi/4$, since the vertical columns should extend beyond the point $x = 1$, where the interface line $y = \sqrt{1 - x^2}$ is not defined. However by combining heights and widths we are able to extend the range of application of the HF method and to minimize the errors in the region $|f^{(1)}(x)| \approx 1$. We have considered about 15 different interface configurations, obtained

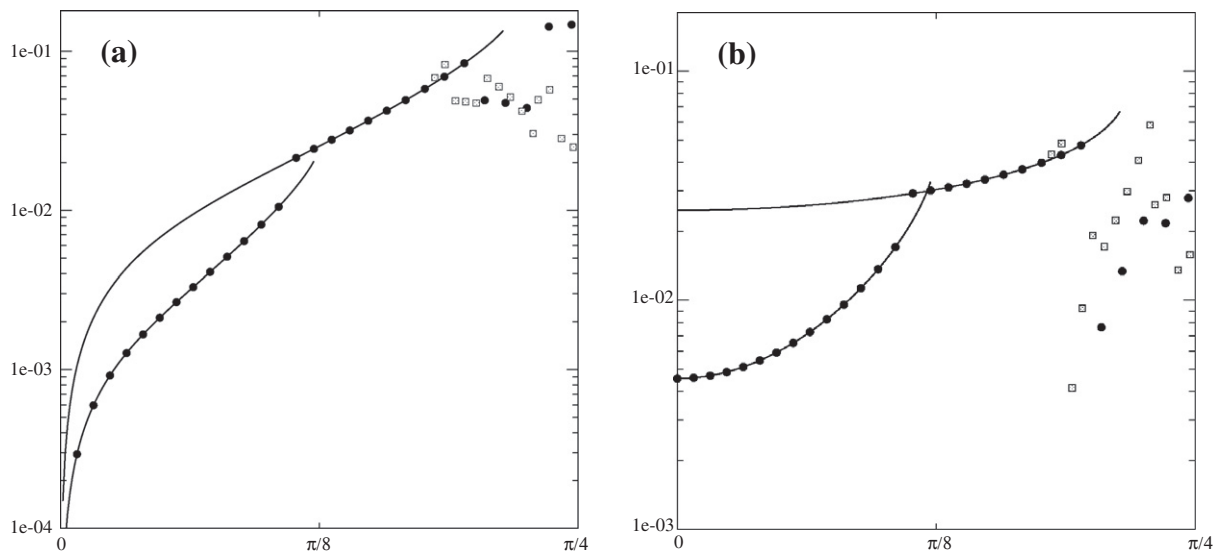


Fig. 7. Analytical errors (thick lines) with the continuous height function for a circle with $r/h = 4$ and $0 \leq \alpha \leq \pi/4$: (a) first derivative; (b) curvature. Top line is second-order accurate, bottom line is fourth-order accurate. Numerical errors from the volume fraction field are at the discrete HF points (full circles) and at the interpolated points (dotted squares).

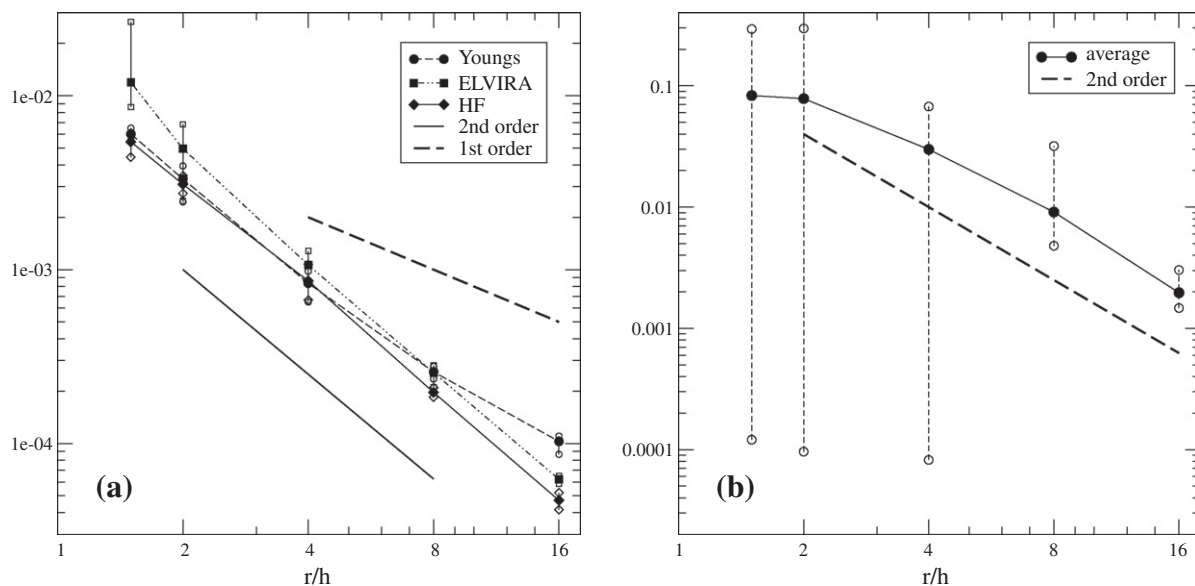


Fig. 8. (a) Convergence of the reconstruction error (24) for a circle with different resolutions, r/h , and algorithms. (b) Convergence of the relative curvature error. In both images are shown average values (full markers) and minimum and maximum values (open markers).

with a horizontal translation of the circle center, to increase the number of points that requires data interpolation near $\alpha = \pi/4$, where the analytical error curves are not defined. The algorithm automatically switches between fourth-order and second-order accuracy and finally to the mixed approach when $\alpha \approx \pi/4$. The numerical errors with the osculating circle approach are clearly bounded.

Finally in Fig. 8 we show how the hierarchical algorithm performs as we increase the resolution from $r/h = 1.5$ up to $r/h = 16$. We have switched off the fourth-order scheme for a direct comparison with other second-order or lower-order algorithms. The reconstruction error defined in (24) has been averaged over 100 circles with the position of the center randomly distributed. In Fig. 8(a) we plot this value together with the minimum and maximum errors computed at each different resolution. The hierarchical algorithm, noted by “HF” in the figure, is competitive with the two other algorithms considered, namely ELVIRA and Parker–Youngs (P–Y), and shows a rather smooth behavior as it switches from the mixed approach to centered finite differences and from a linear to a quadratic interpolation of the geometrical data. In Fig. 8(b) we show the convergence of the relative error norm defined by

$$L_2 = \frac{1}{\kappa} \left(\frac{\sum_i (\kappa_i - \kappa)^2}{\sum_i 1} \right)^{1/2}, \quad (35)$$

where the sum is over all the mixed cells and interface lines and κ is the exact curvature. We also consider the local maximum and minimum absolute value of the relative error. At the lowest resolutions the error is the greatest for the points defined by the Parker–Youngs reconstruction. Furthermore in these cells the Taylor expansion (10) is not valid and the relative error can be of the opposite sign. If the curvature interpolation is required in a point close to where the error changes its sign, then the relative error is indeed very small as seen in Fig. 8(b) at the lowest resolutions. The curvature results are very close to those presented in [17], except that at the lowest resolutions in the present study the error curve levels off because of the osculating circle approximation.

5. Conclusions

We have presented a comprehensive study on the representation of an interface line and its geometrical properties with the height function method in two dimensions. The use of the height function has a twofold advantage: it considers data only on one side of the interface, hence it does not go through the discontinuity of the characteristic function, and by integrating them along one coordinate direction it is smoother than the original volume fraction distribution.

We have shown that the approximation of the derivatives and the curvature based on the height function values are second-order accurate with a three-point stencil, and fourth-order accurate with a five-point stencil, provided the interface line is continuous with its derivatives. We have also shown that the piecewise linear reconstruction converges quadratically with the grid spacing, while the parabolic reconstruction shows a potential third-order convergence rate.

We have presented a hierarchical algorithm that allows the computation of the normal vector and curvature of an interface line with the height function method also when the local radius of curvature is of the order of the grid spacing. At low resolution the algorithm fits the HF values with an approximated osculating circle and data interpolation for the first derivative and curvature is linear. At higher resolution, standard centered finite difference approximations are implemented and data interpolation is quadratic. The numerical results are in agreement with the theory we have presented and show that, when the height function can be defined, the hierarchical algorithm can reconstruct an interface line and calculate its geometrical properties accurately with a smooth transition from fourth- to second-order schemes.

References

- [1] C.W. Hirt, B.D. Nichols, Volume of fluid (VOF) method for the dynamics of free boundaries, *J. Comput. Phys.* 39 (1981) 201–225.
- [2] W.J. Rider, D.B. Kothe, Reconstructing volume tracking, *J. Comput. Phys.* 141 (1998) 112–152.
- [3] R. Scardovelli, S. Zaleski, Direct numerical simulation of free-surface and interfacial flow, *Annu. Rev. Fluid Mech.* 31 (1999) 567–603.
- [4] G. Tryggvason, B. Bunner, A. Esmarelli, D. Juric, N. Al-Rawahi, W. Tauber, J. Han, S. Nas, Y.-J. Jan, A front-tracking method for the computations of multiphase flow, *J. Comput. Phys.* 169 (2001) 708–759.
- [5] C.E. Weatherburn, On differential invariants in geometry of surfaces, with some applications to mathematical physics, *Quart. J. Pure. Appl. Math.* 50 (1925) 230–269.
- [6] D. Gueyffier, J. Li, A. Nadim, R. Scardovelli, S. Zaleski, Volume-of-fluid interface tracking with smoothed surface stress methods for three-dimensional flows, *J. Comput. Phys.* 152 (1999) 423–456.
- [7] J.U. Brackbill, D.B. Kothe, C. Zemach, A continuum method for modeling surface tension, *J. Comput. Phys.* 100 (1992) 335–354.
- [8] I. Aleinov, E.G. Puckett, Computing surface tension with high-order kernels, in: *Proceedings of the 6th International Symposium on Computational Fluid Dynamics, Lake Tahoe, NV, 1995*, pp. 13–18.
- [9] M.W. Williams, D.B. Kothe, E.G. Puckett, Accuracy and convergence of continuum surface tension models, in: W. Shyy, R. Narayanan (Eds.), *Fluid Dynamics at Interfaces*, Cambridge Univ. Press, Cambridge, UK, 1998, p. 294.
- [10] S.J. Cummins, M.M. Francois, D.B. Kothe, Estimating curvature from volume fractions, *Comput. Struct.* 83 (2005) 425–434.
- [11] B.D. Nichols, C.W. Hirt, R.S. Hotchkiss, SOLA-VOF: A solution algorithm for transient fluid flow with multiple free boundaries, Technical Report LA-8355, Los Alamos National Laboratory, 1980.
- [12] J. Helmsen, P. Colella, Non-convex profile evolution in two dimensions using volume of fluids, Technical Report UCRL-ID-126402, Lawrence Livermore National Laboratory, 1997.
- [13] M. Sussman, A second order coupled level set and volume-of-fluid method for computing growth and collapse of vapor bubbles, *J. Comput. Phys.* 187 (2003) 110–136.
- [14] S. Afkhami, M. Bussmann, Height functions for applying contact angles to 2D VOF simulations, *Int. J. Numer. Meth. Fluids* 57 (2007) 453–472.

- [15] M. Sussman, K.M. Smith, M.Y. Hussaini, M. Ohta, R. Zhi-Wei, A sharp interface method for incompressible two-phase flows, *J. Comput. Phys.* 221 (2007) 469–505.
- [16] M. Sussman, M. Ohta, Improvements for calculating two-phase bubble and drop motion using an adaptive sharp interface method, *Fluid Dyn. Mater. Proc.* 3 (2007) 21–36.
- [17] S. Popinet, An accurate adaptive solver for surface-tension-driven interfacial flows, *J. Comput. Phys.* 228 (2009) 5838–5866.
- [18] J.E. Pilliod Jr., E.G. Puckett, Second-order accurate volume-of-fluid algorithms for tracking material interfaces, *J. Comput. Phys.* 199 (2004) 465–502.
- [19] R. Scardovelli, S. Zaleski, Interface reconstruction with least-square fit and split Eulerian–Lagrangian advection, *Int. J. Numer. Meth. Fluids* 41 (2003) 251–274.
- [20] M. Sussman, M. Ohta, High-order techniques for calculating surface tension forces, *Int. Ser. Numer. Math.* 154 (2007) 425–434.
- [21] M.M. Francois, B.K. Swartz, Interface curvature via volume fractions, heights, and mean values on nonuniform rectangular grids, *J. Comput. Phys.* 229 (2010) 527–540.
- [22] P.A. Ferdowsi, M. Bussmann, Second-order accurate normals from height functions, *J. Comput. Phys.* 227 (2008) 9293–9302.
- [23] B.J. Parker, D.L. Youngs, Two and three dimensional Eulerian simulation of fluid flow with material interfaces, Technical Report 01/92, UK Atomic Weapons Establishment, 1992.
- [24] S.V. Diwakar, S.K. Das, T. Sundararajan, A quadratic spline based interface (QUASI) reconstruction algorithm for accurate tracking of two-phase flows, *J. Comput. Phys.* 228 (2009) 9107–9130.
- [25] G. Borgia, Studio dell'approssimazione dell'interfaccia tra due fluidi e delle sue proprietà geometriche con il metodo della funzione altezza, M.S. thesis, Università di Bologna, 2008.